

# SCIENTIFIC REPORTS



OPEN

## Interaction of Sensitizing Dyes with Nanostructured TiO<sub>2</sub> Film in Dye-Sensitized Solar Cells Using Terahertz Spectroscopy

Received: 11 April 2016

Accepted: 29 June 2016

Published: 22 July 2016

William Ghann<sup>1</sup>, Aunik Rahman<sup>2</sup>, Anis Rahman<sup>2</sup> & Jamal Uddin<sup>1</sup>

The objective of this investigation was to shed light on the nature of interaction of different organic dyes and an inorganic dye, Ruthenium (II) polypyridine complex, with TiO<sub>2</sub> nanoparticles. TiO<sub>2</sub> is commonly deployed as an efficient energy transfer electrode in dye sensitized solar cells. The efficiency of dye sensitized solar cells is a function of the interaction of a dye with the electrode material such as TiO<sub>2</sub>. To the best of our knowledge the present study is the first effort in the determination of terahertz absorbance signals, investigation of real-time dye permeation kinetics, and the surface profiling and 3D imaging of dye sensitized TiO<sub>2</sub> films. Herein, we report that the terahertz spectra of the natural dye sensitized TiO<sub>2</sub> films were distinctively different from that of the inorganic dye with prominent absorption of natural dyes occurring at approximately the same wavelength. It was observed that the permeation of the natural dyes were more uniform through the layers of the mesoporous TiO<sub>2</sub> compared to the inorganic dye. Finally, defects and flaws on TiO<sub>2</sub> film were easily recognized via surface profiling and 3D imaging of the films. The findings thus offer a new approach in characterization of dye sensitized solar cells.

Terahertz radiation (T-ray) based spectroscopy employs a range of wavelengths between the microwave and the far-infrared region, from ~10 μm to ~3000 μm. Transient kinetics and different molecular resonances such as vibrational states of materials may be probed with T-rays<sup>1–3</sup>. Terahertz time-domain spectroscopy (THz-TDS) has recently gained attention as a valuable tool for probing molecular transitions that are usually not captured by other spectroscopic techniques such as UV, infrared and Raman spectroscopy<sup>4–6</sup>. The non-ionizing and non-invasive nature of the radiation coupled with its relative transparency to most materials except metals makes it suitable for the analysis of biological structures in their native state.

Another major benefit of THz-TDS is time resolution, which is very important to the dynamics of certain processes, allowing photo-induced responses to be characterized with sub-picosecond temporal resolution<sup>7</sup>. Terahertz spectrometry has been used in a number of applications including the investigation of the permeation kinetics and concentration profile of active ingredients into the human stratum corneum<sup>8</sup>, as well as other biomedical<sup>9,10</sup>, pharmaceutical<sup>11</sup>, proteomics<sup>12,13</sup> and genomics studies<sup>12,13</sup>. Terahertz spectrometry has also been used in the sensing and identification of explosives and other materials of security concerns<sup>14</sup>.

The terahertz portion of the electromagnetic radiation is very sensitive to detailed structural properties as well as charge migration and in recent times have been used to study the photoconductivity and the dynamics of charge separation of several photovoltaic devices<sup>7,10,15–17</sup>. Dye sensitized solar cells (DSSC) are a class of photovoltaic devices that have been widely investigated due to advantages such as ease of fabrication, low cost, ecofriendly nature and appreciable solar-to-electric energy conversion efficiency<sup>18–20</sup>. DSSC comprises of a photoanode, an electrolyte system for charge regeneration and a counter electrode. The present work focuses on the photoanode which consist of a transparent conducting oxide (typically Indium doped Tin Oxide, ITO, or Fluorine doped Tin Oxide, FTO) substrate covered with a thin film of titanium dioxide (TiO<sub>2</sub>) nanoparticles, and a dye<sup>21</sup>. The dye is used to sensitize the wide band gap TiO<sub>2</sub> electrode. Upon illumination by solar energy, dye molecules absorb photons and move to the excited states. The excited electrons are subsequently injected into the TiO<sub>2</sub> conduction

<sup>1</sup>Center for Nanotechnology for Department of Natural Sciences, Coppin State University, 2500 W. North Avenue, Baltimore, MD 21216, USA. <sup>2</sup>Applied Research & Photonics, 470 Friendship Road, Suite 10, Harrisburg, PA 17111, USA. Correspondence and requests for materials should be addressed to J.U. (email: juddin@coppin.edu)

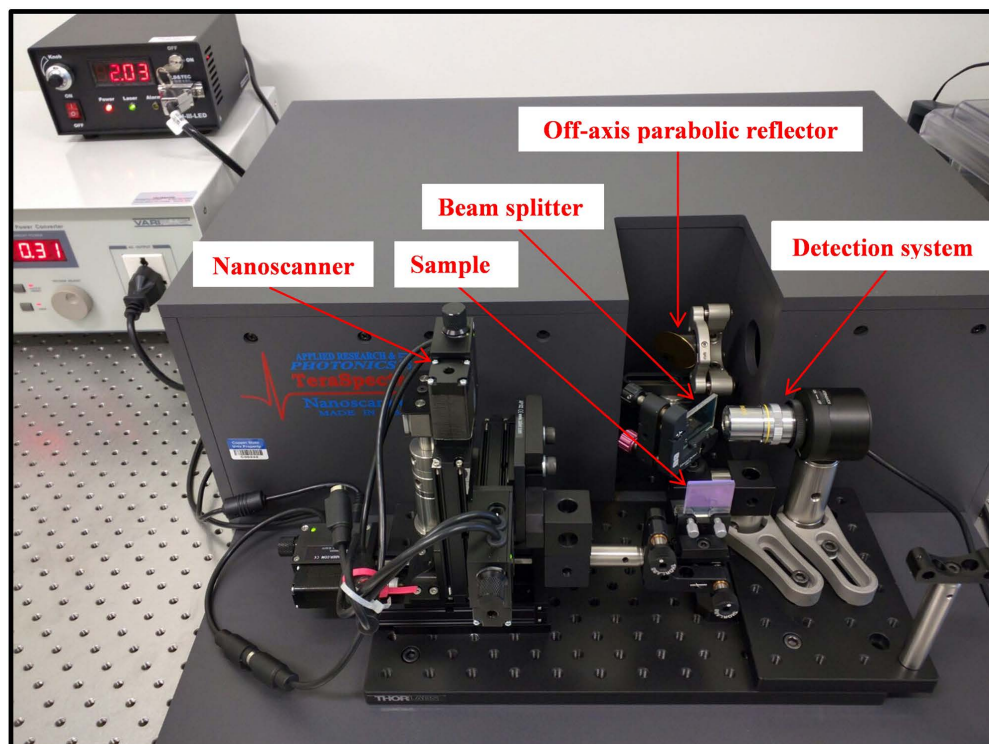


**Figure 1.** Pomegranate sensitized  $\text{TiO}_2$  slide mounted on the XYZ-stage in the Terahertz probe setup.

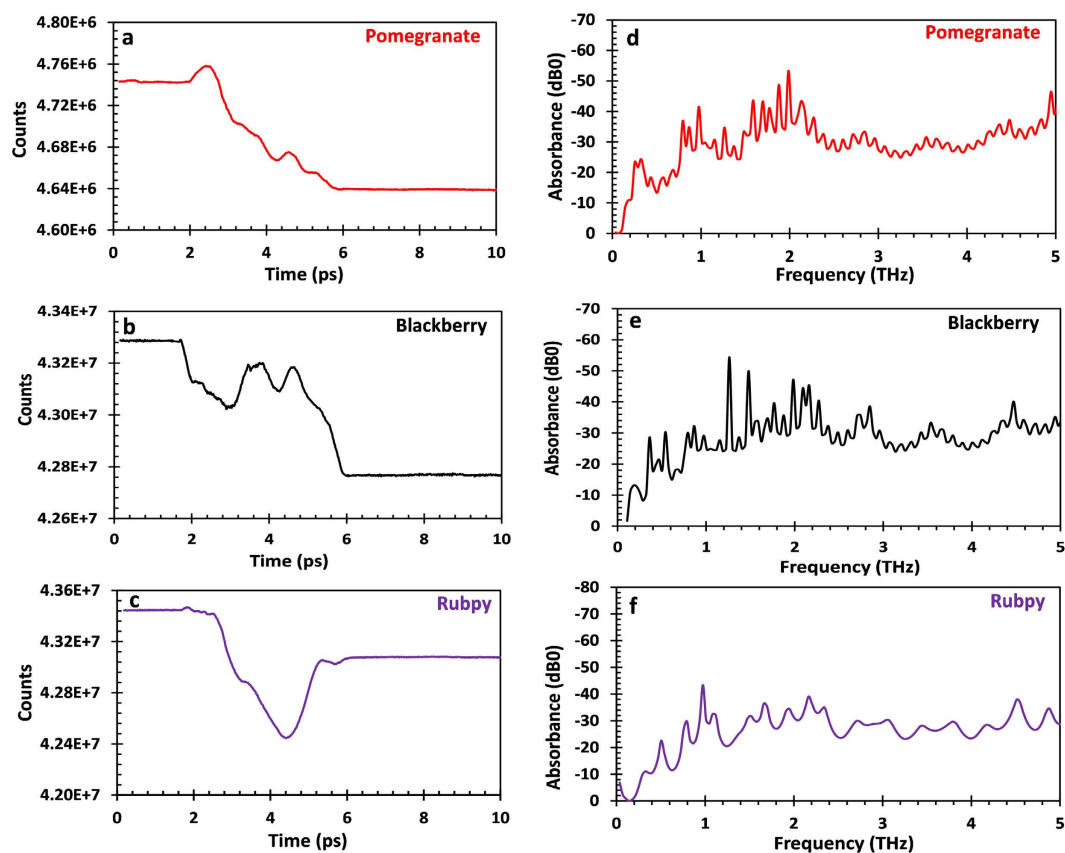


**Figure 2.** Time-domain temporal signal (a–c); its corresponding Fourier transform broadband terahertz absorbance spectra (d–f) of pomegranate (a,d) blackberry (b,e) and Rubpy (c,f) dye sensitized  $\text{TiO}_2$  on FTO glass.

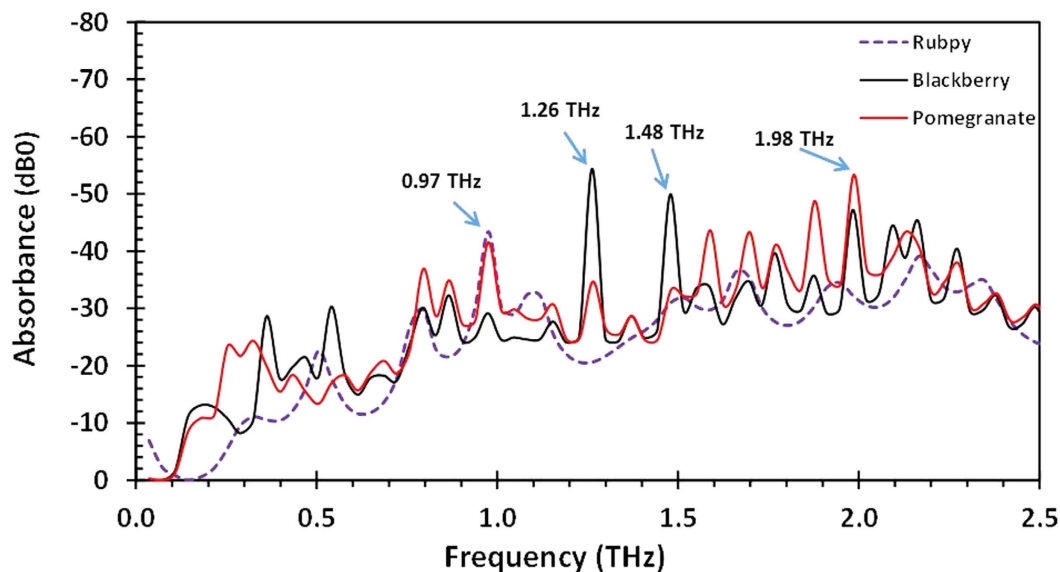


**Figure 3.** Fourier transform frequency spectra of three different dye sensitized  $\text{TiO}_2$  films (pomegranate, blackberry and Rubpy) showing distinct absorbance characteristics.

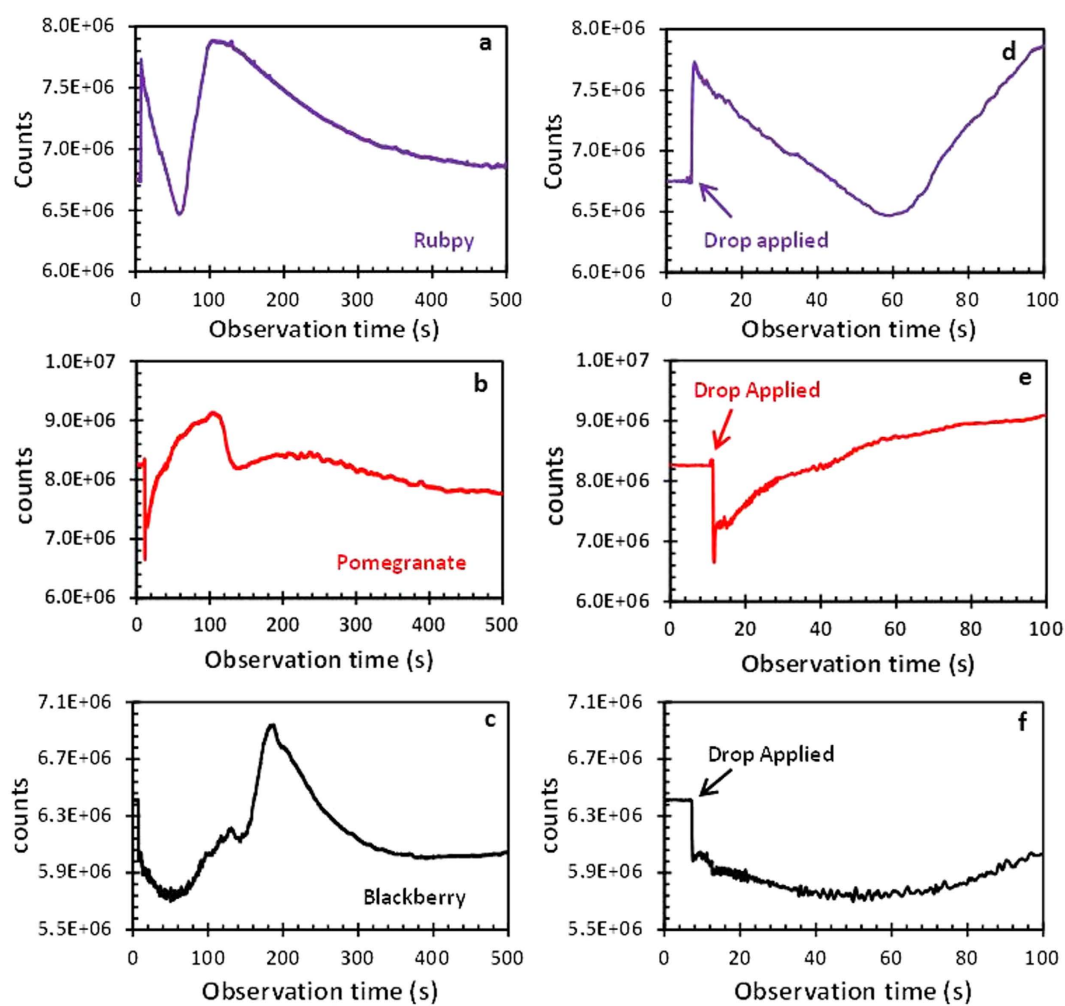


**Figure 4.** Kinetics of permeation of three different dyes into  $\text{TiO}_2$  films coated on FTO glass: (a) Rubpy; (b) pomegranate; (c) blackberry. Close-up view: (d) Rubpy; (e) pomegranate; (f) blackberry.

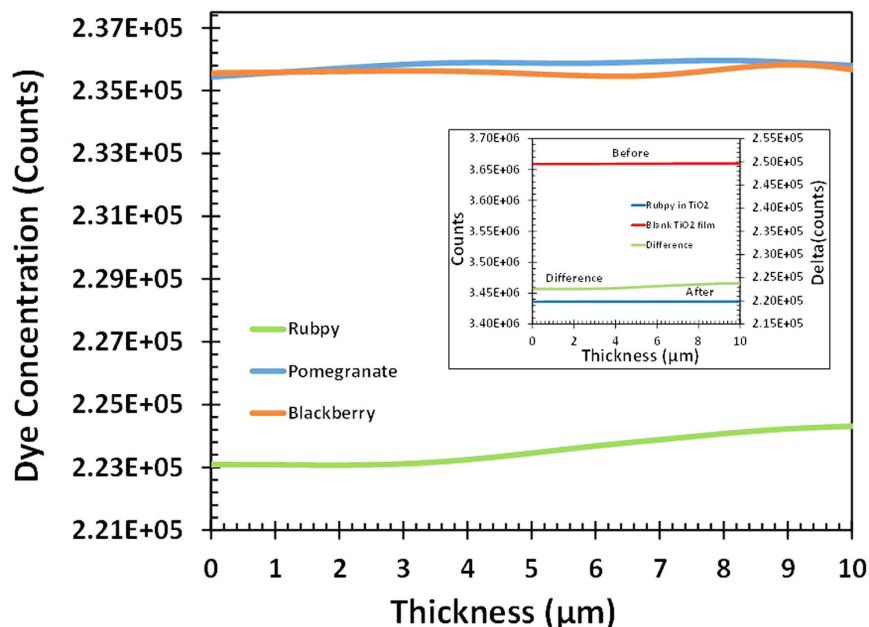


**Figure 5.** Diffusion characteristics of Rubpy, pomegranate, and blackberry dyes in mesoporous TiO<sub>2</sub>; (inset) Depth scan of Rubpy dye sensitized TiO<sub>2</sub> film. Top (red) scan of blank TiO<sub>2</sub> film and bottom (blue) is the scan after the TiO<sub>2</sub> is saturated with Rubpy dye. The middle curve (green, right axis) is the difference of the top and the bottom curves, indicating the distribution of the Rubpy dye across TiO<sub>2</sub> film.

band. An injected electron diffuses through the nanocrystalline TiO<sub>2</sub> to the conductive film and then transferred to an external circuit<sup>22–24</sup>. An in-depth understanding of the interaction of dyes with the electron-transporting TiO<sub>2</sub> electrodes will form the basis for further research that will improve our understanding of the mechanisms of charge generation and transport leading up to the production of electrical energy. A number of studies have been carried out to investigate the influence of dye sensitization on the overall efficiency of solar cells<sup>25–28</sup>.

In the present paper, T-rays have been used to investigate the interaction properties of the photoanode component of the solar cell and could provide information on any defects that can potentially affect the overall efficiency of dye sensitized solar cells. The TiO<sub>2</sub> film provides an efficient scaffold to hold large amount of dye molecules needed for light harvesting. However, if there are cracks in this scaffold, it reduces the number of dye molecules adsorbed on the TiO<sub>2</sub> and thus subsequently affect the efficiency of the solar cell. A means to detect cracks and flaws in the TiO<sub>2</sub> film and consequently the dye sensitized solar cell will thus help improve the fabrication of high performance dye sensitized solar cells. The three dyes chosen for the studies were two different organic (pomegranate and blackberry dye) and an inorganic dye, Ruthenium (II) polypyridine complex (Rubpy). The three dyes were chosen mostly on the account of their strong absorption properties. Rubpy complexes are the most common type of dye utilized in the fabrication of dye sensitized solar cells<sup>29</sup>. Blackberry and Pomegranate, like other natural dyes used in solar cell fabrication, have appreciable light absorption properties and preferable in terms of their ecofriendly nature, low cost and abundance<sup>30–32</sup>. The various anchoring groups on the dyes provide means of attachment to the TiO<sub>2</sub> surface. Herein is reported terahertz reflectometry and spectrometry studies on dye sensitized titanium dioxide coated FTO glass plates commonly used in the fabrication of DSSC. Terahertz measurements were carried out using a terahertz time-domain spectrometer with an attached nanoscanner as displayed in Fig. 1. The spectral features of the dyes adsorbed on TiO<sub>2</sub> were studied using THz-TDS techniques and its characteristic spectra ranging from 0 to 5 THz were obtained. A fast and effective methodology was developed for the inspection and identification of defects on solar cells.

## Results and Discussion

**Spectroscopic Studies of Dye Sensitized TiO<sub>2</sub> films.** Teraspectra has been shown to be very sensitive to various resonances in number of different molecules<sup>4,5</sup>. Many materials exhibit distinct spectral absorption features in the THz range of the electromagnetic spectrum and this makes possible the identification and characterization of such materials<sup>33,34</sup>. Terahertz radiation is sensitive to the vibrational states of an entire molecule and terahertz spectra, accordingly, corresponds to molecular or inter-molecular behavior and provides information unique to a given molecule or substance. As a result, no two molecules exhibit exactly identical terahertz absorbance peaks as it is in the case of mid-infrared spectra which give intra-molecular information<sup>5</sup>. Light absorption by dye sensitized TiO<sub>2</sub> coated FTO plates were investigated with the terahertz probe pulses. The terahertz characteristic absorption spectra were obtained in the range of 0–35 THz. However, for the reason that too many peaks placed on a single plot makes the plot very busy, only data in the range of 0–5 THz are reported in this paper. The THz-TDS spectrometer generates data first in the time domain to which Fourier transform algorithms is applied to obtain a frequency spectrum. Figure 2a–c exhibits the time-domain pulses (or interferogram) of the three dyes studied. Although T-ray provides information about the entire molecule it could be seen that the interferogram

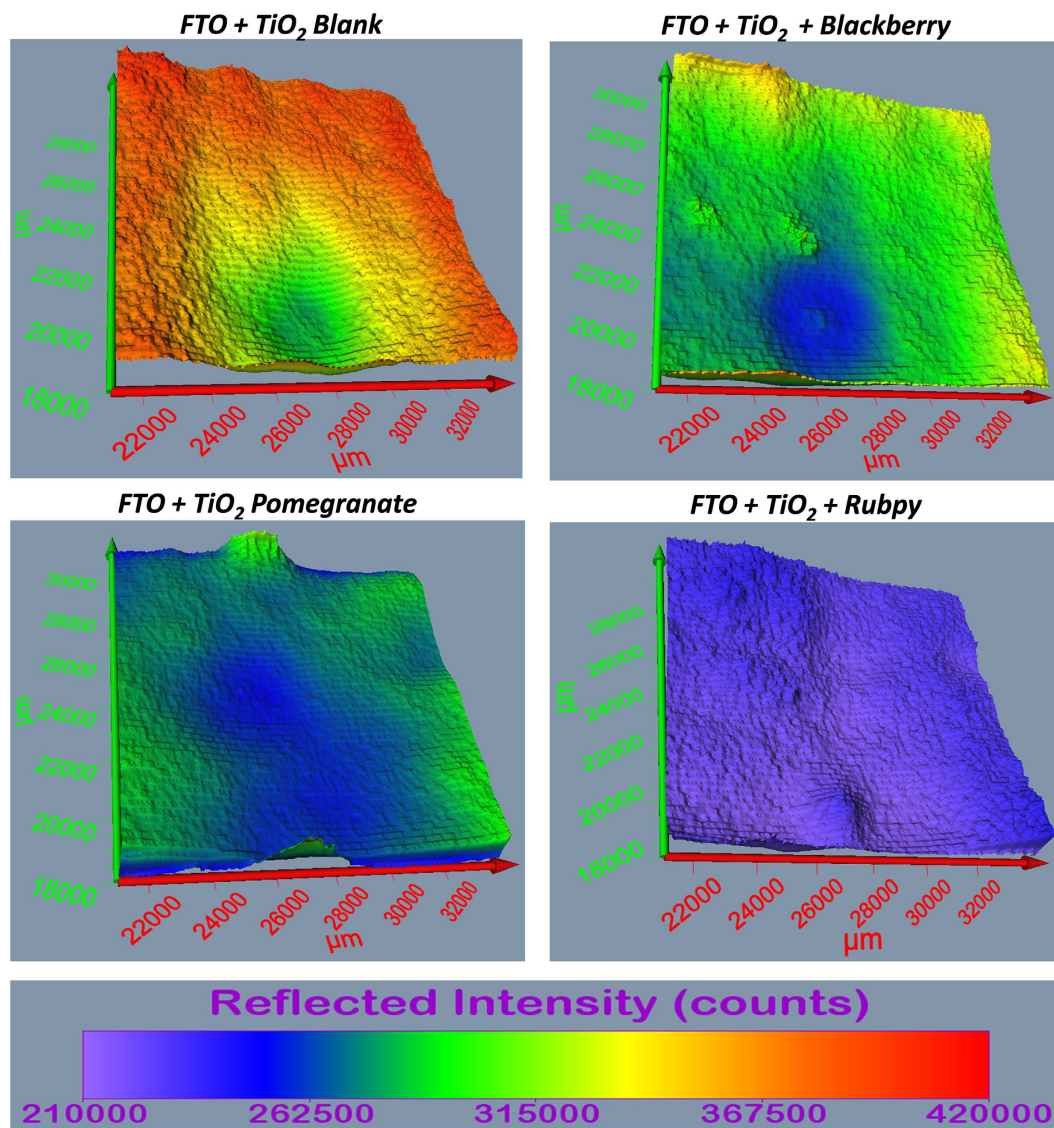


**Figure 6.** Comparison of the surface plot of blank  $\text{TiO}_2$ , blackberry, pomegranate and Rubpy dye sensitized  $\text{TiO}_2$  film coated on FTO glass (Size of film scanned  $\sim 13000 \times 13000 \mu\text{m}^2$ ).

of the natural dyes (Fig. 2a,b) follow the same trend as opposed to the inorganic dye. The time-domain signal in Fig. 2a–c were Fourier transformed to obtain the terahertz spectra in Fig. 2d–f. The terahertz spectral features obtained for the natural dyes were very similar to each other and had a lot of overlapping peaks when the three spectra were displayed together in Fig. 3.

Pomegranate dye sensitized  $\text{TiO}_2$  films exhibited prominent absorption peaks at 0.33 THz, 0.97 THz, 1.99 THz, 2.85 THz, 3.54 THz and 4.48 THz. Blackberry dye sensitized  $\text{TiO}_2$  on the other hand exhibited prominent absorption peaks at 0.54 THz, 1.3 THz, 2.0 THz, 2.8 THz, 3.5 THz and 4.5 THz. The overlay of the spectra of all three dyes in Fig. 3 shows that the absorption characteristics of the natural dyes are very similar: the absorption peaks overlap with each other and are much sharper than the peaks of the Rubpy sensitized films. Rubpy sensitized  $\text{TiO}_2$  films had only high absorption peak at 0.97 THz which was comparable to that of pomegranate and blackberry dye sensitized  $\text{TiO}_2$  films.

**Kinetic Studies of Dye Sensitized  $\text{TiO}_2$  films.** Kinetic studies were conducted on the three dye sensitized  $\text{TiO}_2$  films to evaluate the rate at which the dyes diffuse through the  $\text{TiO}_2$  nanoparticle matrix. Aliquot  $20 \mu\text{L}$  of the dye was dropped on the film and the transient kinetics of diffusion of the dyes was recorded over a period of 500 seconds as the dyes permeated the titanium dioxide film. Figure 4 exhibits the characteristics of diffusion of the respective dyes in titanium dioxide substrate. With all the dyes, there is an initial broad decrease in intensity counts followed by an increase in intensity counts before they level off. Based on the slope of the curves in the first 100 seconds, Rubpy seems to have the fastest kinetics, reaching the peak of its intensity counts within 40 seconds after the initial drop in intensity. After this increase in transmitted intensity, there is a gradual decrease in intensity until it reaches a plateau. Rapid evaporation of the dye during the measurement, which most likely exposes some

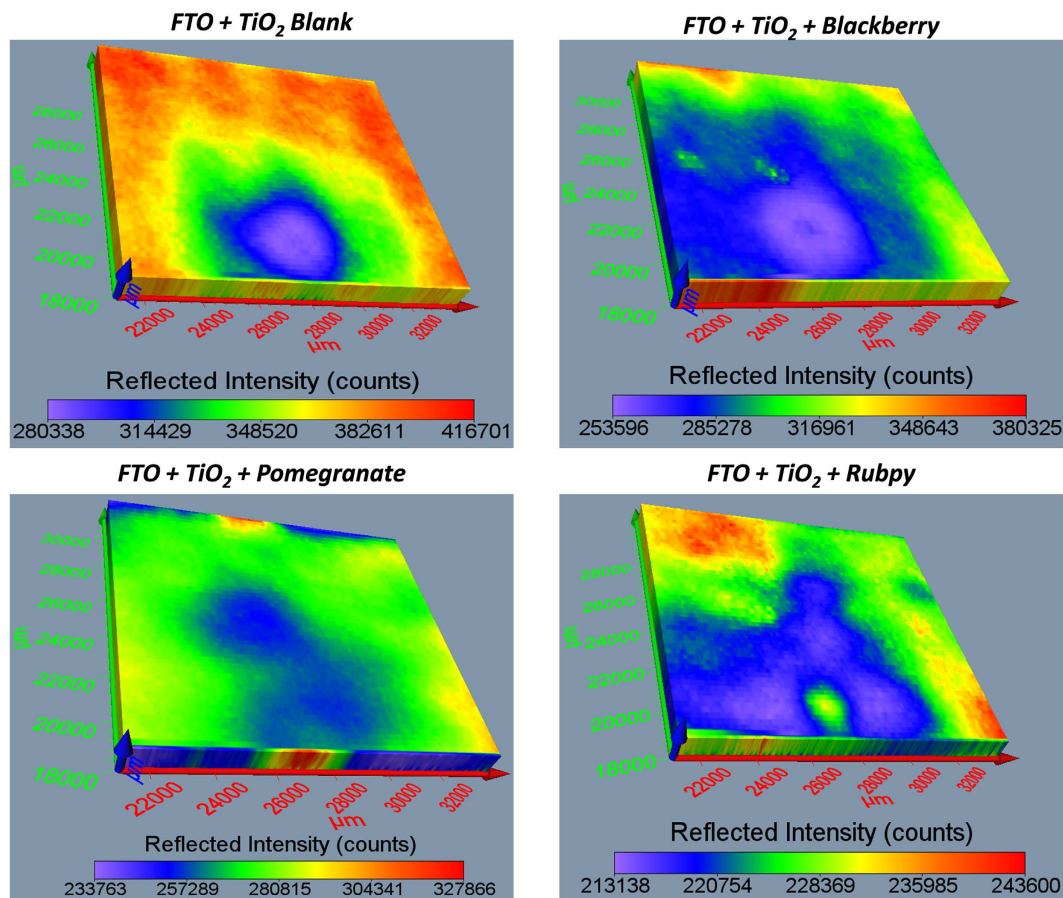


**Figure 7.** Comparison of the 3D images of blank  $\text{TiO}_2$  blackberry, pomegranate and Rubpy dye sensitized  $\text{TiO}_2$  coated FTO film (Size of sample scanned  $\sim 13000 \times 13000 \mu\text{m}^2$ ).

part of the titanium dioxide nanoparticles, could account for this sudden increase in intensity. Unlike pomegranate and blackberry dyes which were used in their natural form, Rubpy solution was prepared by dissolving the solid form in a suitable amount of deionized water and this could account for the rapid diffusion rate. After the initial decrease in intensity upon application of the pomegranate dye, there is a gradual increase in intensity from 12 seconds after dye application to about 100 seconds after dye application. The intensity counts subsequently decreases till it levels off. Blackberry dye has the slowest kinetics; after the initial drop in intensity counts upon application of dye, it takes over 100 seconds to reach the maximum intensity and then steadily decrease in intensity till it reaches a plateau. Rubpy diffusion reached saturation faster than both of the natural dyes as indicated by flattening of its slope. Figure 4d–f shows a close-up of Fig. 4a–c where the X-axis is zoomed to 100 seconds. It can be observed that the inorganic dye (Rubpy) shows an initial transmission count higher than that of FTO/ $\text{TiO}_2$  substrate alone whereas pomegranate and blackberry show a decrease in intensity before slowly going up in intensity count. This may be indicative of the fact that each of these dyes interact with the  $\text{TiO}_2$  nanoparticles in their own unique way. Further investigation will be conducted for conclusive remarks on this observation.

**Depth Scan Measurement of Dye Sensitized  $\text{TiO}_2$  films.** The Terahertz scanning reflectometry was used to assess the concentration profile of the different dyes into the  $\text{TiO}_2$  film. The technique has been previously used to investigate the concentration profile of the active ingredients across the stratum corneum of the skin<sup>8</sup>. Depth scan of  $\text{TiO}_2$  films before and after saturation with the various dyes was carried out to assess their reflectance at increasing depth and thereby understand the distribution of the dye in the titanium dioxide mesoporous film. The scanning measurement was first carried out on the blank FTO/ $\text{TiO}_2$  film, as a control, after which 20  $\mu\text{L}$  of dye was applied and allowed to fully saturate the  $\text{TiO}_2$  layer. All the measurements were carried out under identical conditions. A second scanning measurement was carried out after  $\text{TiO}_2$  was fully saturated with the dye. The film was considered fully saturated when kinetics of the dye reached a steady state. The difference in reflectance intensity of the FTO/ $\text{TiO}_2$  film saturated with the dye offers insight into the concentration of the dyes across the depth of the  $\text{TiO}_2$  film. The intensity of terahertz radiation through a portion of the glass substrate was also measured since it is dependent on the amount of light adsorbed in the Dye/ $\text{TiO}_2$  film. Figure 5 (inset) shows the computation of the amount of Rubpy dye (green curve) from the scan of the blank (red curve) and saturated substrate (blue curve). The result of the measurements as displayed in Fig. 5 show that the concentration of Rubpy in the  $\text{TiO}_2$  is not uniform indicated by the increase in intensity with increasing depth of the mesoporous film. Conversely, the permeation of the natural dyes are uniform through all the layers of the mesoporous  $\text{TiO}_2$  film.

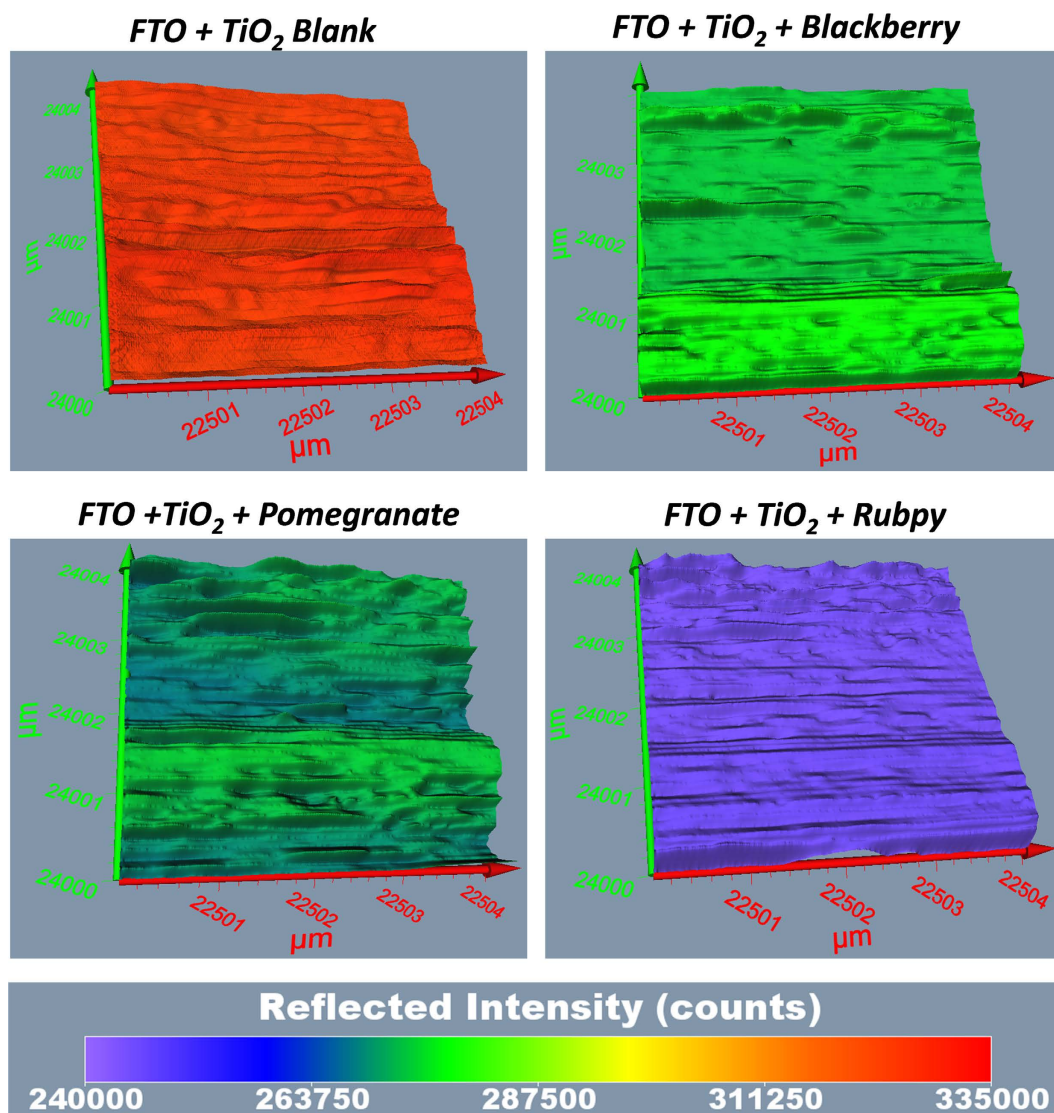


**Figure 8.** Comparison of the surface plot of blackberry, pomegranate and Rubpy dye sensitized  $\text{TiO}_2$  film coated on FTO glass with their corresponding blank  $\text{TiO}_2$  film coated on FTO glass. (Size of sample scanned  $\sim 4 \times 4 \mu\text{m}^2$ ).

The concentration of blackberry dye is, however, relatively more constant through the layers. This result corroborates with that of the kinetic study (Fig. 4) which shows Rubpy to have the fastest kinetics and blackberry dye with the lowest kinetics. It can be deduced that the slower the kinetics the more uniform the concentration of the dye across the depth of the substrate.

**Surface Profiling and 3D Imaging of Dye Sensitized  $\text{TiO}_2$  films.** The Terahertz scanning reflectometry has shown promise as an important tool for obtaining tomographic information of the surface, subsurface, and interaction of the constituents of a specimen. The Terahertz subsurface imaging was carried out to examine nanoscopic features of  $\text{TiO}_2$  before and after the application of various dyes. Two different  $\text{TiO}_2$  film sizes were scanned:  $13000 \times 13000 \mu\text{m}^2$  area (Figs 6 and 7) to give a general overview of the sample film and  $4 \times 4 \mu\text{m}^2$  area (Figs 8 and 9) to obtain detailed features of the film. The surface plots (Figs 6 and 8) and 3D images (Figs 7 and 9) were obtained for blank substrate ( $\text{TiO}_2$  alone); to serve as a control, and pomegranate, blackberry and Rubpy dye diffused  $\text{TiO}_2$  film. The sizes of  $\text{TiO}_2$  films measured in microns are indicated on the coordinate axes.

In Figs 6 and 8, the intensity of reflected light is normalized for the blank  $\text{TiO}_2$  and all the dye sensitized  $\text{TiO}_2$  films for easy visual comparison of the degree to which each sample film reflect light. The intensity of reflected light in Figs 7 and 9 on the other hand is not normalized for all the sample films and thus provide information about the relative intensities of the different parts of a given sample film. It was observed from all the measurements that the intensities of reflected light were not only based on the permeation of the dyes into  $\text{TiO}_2$  film but also due in part to the thickness and morphology of the blank  $\text{TiO}_2$  film. Thin or exposed surfaces of the film produced high intensity of reflected light whereas crests and ridges exhibited low intensity of reflected light.

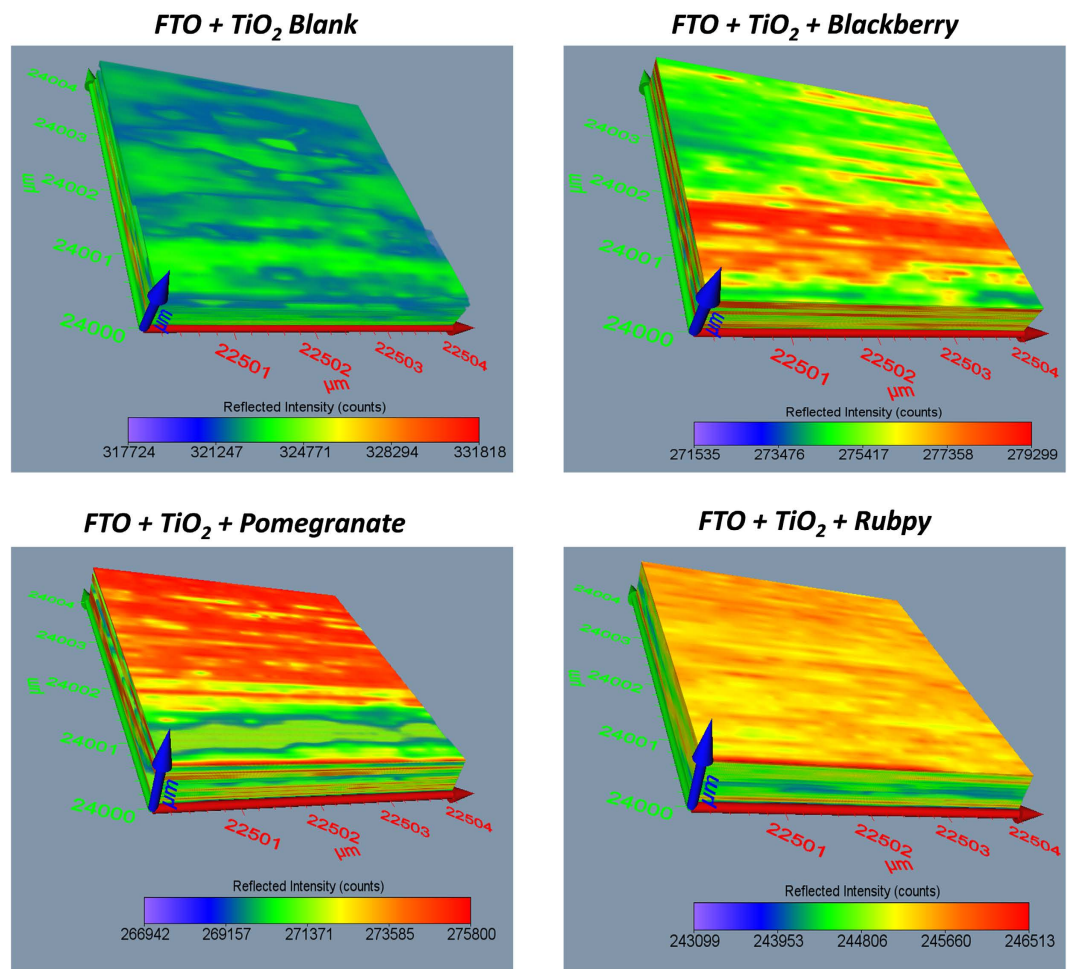


**Figure 9.** Comparison of the 3D images of blackberry, pomegranate and Rubpy dye sensitized  $\text{TiO}_2$  film coated on FTO glass with their corresponding blank  $\text{TiO}_2$  coated on FTO glass. (Size of film scanned  $\sim 4 \times 4 \mu\text{m}^2$ ).

The reconstructed surface plots (Figs 6 and 8) clearly revealed exposed surfaces and defects present on the dye sensitized  $\text{TiO}_2$  coated FTO glass substrate. A thicker spot near the center of the mesoporous  $\text{TiO}_2$  film created in the process of spinning  $\text{TiO}_2$  paste on the FTO glass slides showed up as an artifact on the surface plot of the blank  $\text{TiO}_2$  and all three dye sensitized  $\text{TiO}_2$  films. Some spots of the  $\text{TiO}_2$  film got detached from the FTO glass on application of the dye resulting in higher intensity of reflected light as seen for Rubpy in Fig. 6. This is indicative of a spin/dye dropping related change of the  $\text{TiO}_2$  film. The thicker spots are less obvious in the  $4 \times 4 \mu\text{m}^2$  film size scan (Fig. 8) since the scan was performed outside of the main area with artifact.

The artifact was also visible on the 3D images (Fig. 7) and more prominently in Rubpy sensitized  $\text{TiO}_2$  film where the exposed glass in the center of artifact is signified by high intensity of reflected light. A careful examination of 3D reconstructed image of the Rubpy sensitized  $\text{TiO}_2$  film (Fig. 7) shows a complete saturation of the dye in the  $\text{TiO}_2$  matrix. The patches of light blue color may indicate dye evaporated from the surface of the  $\text{TiO}_2$ . The permeation characteristic of blackberry dye is similar to that of pomegranate (Figs 6 and 8). The intensity of reflected light is low at the point of application of the dye but increases outwardly.

**Detection of Defects Present of Dye Sensitized  $\text{TiO}_2$  Films.** To confirm the unique capability of Terahertz reflectometry to detect flaws present on the dye sensitized  $\text{TiO}_2$  films. A  $10 \text{ mm} \times 23 \text{ mm}$  portion of  $25 \text{ mm} \times 25 \text{ mm}$  dye sensitized  $\text{TiO}_2$  films were scanned to detect any defects present on the films. Pomegranate, blackberry and Rubpy dye sensitized solar cell electrodes were scanned and with the measurements, 3-D images, comparable to scanning electron microscopy images, were generated. As displayed in Fig. 10, the cracks present in the  $\text{TiO}_2$  films show up as large peaks on the surface plots due to the greater intensity of reflected light from the exposed glass surface. The magnitude of the peaks correlate with the size of the exposed surface area. Defects are easily noticeable as they reflect more light. As displayed in Fig. 10, the protruding peaks in blackberry dye sensitized  $\text{TiO}_2$  film (Fig. 10a) and pomegranate dye sensitized  $\text{TiO}_2$  film (Fig. 10b) are bigger than that of Rubpy dye sensitized  $\text{TiO}_2$  film (Fig. 10c). These defects are not so much as a result of the dye application as it is the result of the lack of uniformity of the layer of  $\text{TiO}_2$  on the glass substrate. The results demonstrate the unique defect detection capabilities of Terahertz reflectometry and how it is well suited to efficiently detect flaws and malfunctioning areas of solar cells.

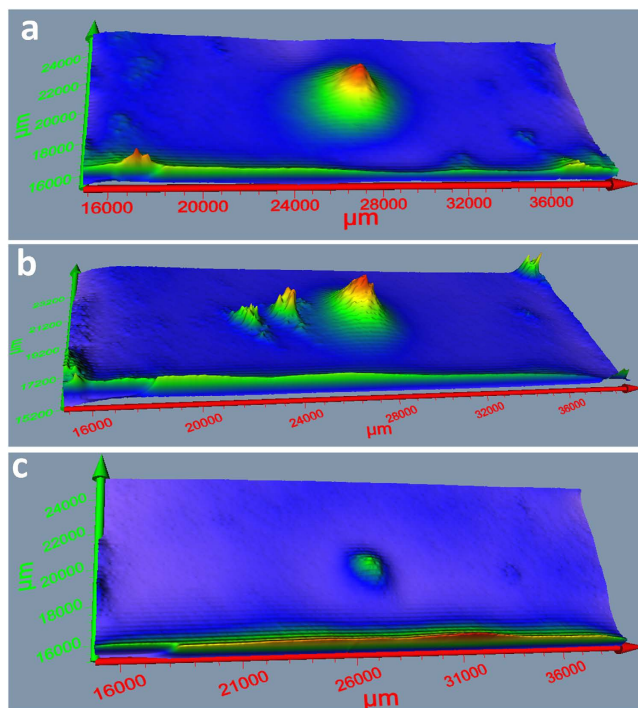


**Figure 10.** 10 mm × 23 mm Surface plots showing defects on dye sensitized TiO<sub>2</sub> films: (a) blackberry; (b) pomegranate; (c) Rubpy.

## Conclusion

Terahertz spectrometry was used to study and characterize the interaction of two organic dyes (pomegranate and blackberry) and an inorganic dye, Ruthenium (II) polypyridine complex (Rubpy) with mesoporous TiO<sub>2</sub>. A spectroscopic analysis exhibited similar terahertz absorbance peaks for the organic dye sensitized TiO<sub>2</sub> films which were different from the peaks of the inorganic dye sensitized TiO<sub>2</sub> films. Diffusion kinetics and concentration distribution profile of the applied dye into the TiO<sub>2</sub> matrix revealed that Rubpy has the fastest kinetics and blackberry dye has the slowest kinetics. In contrast to the inorganic dye, the organic dyes were uniform through the layers of the mesoporous TiO<sub>2</sub>. Surface profiling and 3D imaging of dye sensitized TiO<sub>2</sub> films revealed unevenness and flaws present on the film and thus demonstrated the unique defect detection capability of Terahertz reflectometry. Terahertz spectrometry thus provides an effective means to optically measure dye sensitized TiO<sub>2</sub> electrode properties prior to the fabrication of DSSC.

## Experimental Methods

**Time-domain terahertz spectrometer.** Terahertz measurements were carried out using a terahertz time-domain spectrometer with an attached nanoscanner (TeraSpectra, Applied Research & Photonics, and Harrisburg, PA). The spectrometer portion is similar to a setup described previously<sup>5</sup>. Briefly; an electro-optic dendrimer is excited by a pump laser, where continuous wave (CW) terahertz radiation is generated via a mechanism called dendrimer dipole excitation (DDE). This DDE source generates stable terahertz radiation over a range of ~0.1 THz to ~30 THz at room temperature. The measurements are carried out in either a spectrometer mode, for insight into molecular transition within a sample, or in a reflection mode for surface profiling and 3D imaging. The navigation between the two modes is facilitated by a nanoscanner component of the instrument. The nanoscanner position samples in the beam path for transmission measurements and also allows the scanning of samples in three dimensions to probe the inner layers.

Figure 1 shows the TeraSpectra with the reflection module and a sample (pomegranate dye sensitized TiO<sub>2</sub> film on FTO glass) mounted on the sample holder. During 3D imaging measurements, the terahertz beam first hit the off-axis parabolic reflector and is focused on the sample at a 90 degree angle. The reflected beam from the sample is directed to the detection system via the beam splitter as illustrated in Fig. 1 and Supplementary Figure S1. 3D motion of the sample holder is facilitated by the nanoscanner enabling the interrogation of the reflectance across all the three axis of the sample. Supplementary Figure S1 is a schematic set-up of terahertz scanning reflectometry used for permeation kinetics and concentration profile of the dye in the sub surface of dye sensitized titanium dioxide films.

**Materials.** The transparent conductive oxide coated polymer, FTO (1" × 1" or 2.5 cm × 2.5 cm) with coating thickness of 4,000 Angstrom was purchased from Hartford Glass Co. Inc. Titanium Dioxide Power (Degussa P25) was procured from the institute of chemical education. Fresh fruit of pomegranate and blackberry, purchased in Baltimore, were peeled and their dye extracted with a commercial juicer.

**Sample Preparation.** The FTO coated conductive glass served as the substrate for the preparation of the samples. TiO<sub>2</sub> paste, prepared according to a previously published procedure<sup>35</sup>, was spread uniformly across the conductive side of the glass using a spin coater. The TiO<sub>2</sub> films were subsequently placed on a hot plate with a surface temperature of 380 °C to anneal for over a period of 6 hours. They were then cooled down to room temperature before the application of the freshly prepared dye. For spectral measurements and 3D imaging, the TiO<sub>2</sub> films were immersed in the dye solution overnight and then rinsed with water and acetone before measurement. Supplementary Figure S4 shows a schematic of the stages involved in the fabrication of the solar cells. For kinetic studies, aliquot 20 μL of the respective dye was measured with a micropipette and dropped directly over TiO<sub>2</sub> coated FTO film right before measurement.

**Data Analysis.** The experimental data obtained in time-domain signal (interferogram or terahertz pulse) were analyzed using the Fourier transform of unevenly sampled data algorithm via commercially available software package AutoSignal<sup>®</sup> v. 1.7 by SeaSolve Software Inc. The surface plots and 3D images were generated by means of voxler<sup>®</sup> 3 visualization software from Golden Software Inc. The data for kinetic studies were analyzed via Microsoft Excel 2013.v.

## References

1. Tonouchi, M. Cutting-edge terahertz technology. *Nat Photon* **1**, 97–105 (2007).
2. McIntosh, A. I., Yang, B., Goldup, S. M., Watkinson, M. & Donnan, R. S. Terahertz spectroscopy: a powerful new tool for the chemical sciences? *Chem. Rev.* **41**, 2072–2082 (2012).
3. Beard, M. C., Turner, G. M. & Schmittenmaer, C. A. Terahertz Spectroscopy. *J. Phys. Chem* **106**, 7146–7159 (2002).
4. Rahman, A. Terahertz Spectrometry and Reflectometry: A New Frontier for Noninvasive Picoscale Investigations. *Spectroscopy* **28**, 44–53 (2013).
5. Rahman, A. Dendrimer based terahertz time-domain spectroscopy and applications in molecular characterization. *J. Mol. Struct.* **1006**, 59–65 (2011).
6. Schmittenmaer, C. A. Exploring Dynamics in the Far-Infrared with Terahertz Spectroscopy. *Chem. Rev.* **104**, 1759 (2004).
7. Nemes, C. T., Koenigsmann, C. & Schmittenmaer, C. A. Functioning Photoelectrochemical Devices Studied with Time-Resolved Terahertz Spectroscopy. *J. of Phys. Chem. Lett.* **6**, 3257–3262 (2015).
8. Rahman, A. *et al.* Diffusion Kinetics & Permeation Concentration of Human Stratum Corneum Characterization by Terahertz Scanning Reflectometry. *Drug Dev. Del.* **12**, 43–49 (2012).
9. Bakopoulos, P. *et al.* A tunable continuous wave (CW) and short-pulse optical source for THz brain imaging applications. *Mea. Sci. Technol.* **20**, 104001 (2009).
10. Joseph, C. S., Yaroslavsky, A. N., Neel, V. A., Goyette, T. M. & Giles, R. H. Continuous wave terahertz transmission imaging of non-melanoma skin cancers. *Lasers Surg. Med* **43**, 457–462 (2011).
11. Sibik, J., Löbmann, K., Rades, T. & Zeitler, J. A. Predicting Crystallization of Amorphous Drugs with Terahertz Spectroscopy. *Mol. Pharm.* **12**, 3062–3068 (2015).
12. Plusquellic, D. F., Siegrist, K., Heilweil, E. J. & Esenturk, O. Applications of terahertz spectroscopy in biosystems. *Chemphyschem* **8**, 2412–2431 (2007).
13. Kutteruf, M. R. *et al.* Terahertz spectroscopy of short-chain polypeptides. *Chem. Phys. Lett.* **375**, 337–343 (2003).
14. Liu, H. B., Zhong, H., Karpowicz, N., Chen, Y. & Zhang, X. C. Terahertz Spectroscopy and Imaging for Defense and Security Applications. *Proc. of the IEEE* **95**, 1514–1527 (2007).
15. Brauer, J. C., Marchioro, A., Paraecattil, A. A., Oskouei, A. A. & Moser, J.-E. Dynamics of Interfacial Charge Transfer States and Carriers Separation in Dye-Sensitized Solar Cells: A Time-Resolved Terahertz Spectroscopy Study. *J. Phys. Chem. C* **119**, 26266–26274 (2015).
16. Hendry, E., Koeberg, M., O'Regan, B. & Bonn, M. Local Field Effects on Electron Transport in Nanostructured TiO<sub>2</sub> Revealed by Terahertz Spectroscopy. *Nano Lett.* **6**, 755 (2006).
17. Němec, H., Kužel, P. & Sundström, V. Charge transport in nanostructured materials for solar energy conversion studied by time-resolved terahertz spectroscopy. *J. Photochem. Photobiol. A* **215**, 123 (2010).
18. O'Regan, B. & Grätzel, M. A low-cost, high-efficiency solar cell based on dye-sensitized colloidal TiO<sub>2</sub> films. *Nature* **353**, 737–740 (1991).
19. Cherepy, N. J., Smestad, G. P., Grätzel, M. & Zhang, J. Z. Ultrafast Electron Injection: Implications for a Photoelectrochemical Cell Utilizing an Anthocyanin Dye-Sensitized TiO<sub>2</sub> Nanocrystalline Electrode. *J. Phys. Chem.* **101**, 9342–9351 (1997).
20. Hagfeldt, A., Boschloo, G., Sun, L., Kloo, L. & Pettersson, H. Dye-Sensitized Solar Cells. *Chem. Rev.* **110**, 6595 (2010).
21. Shalini, S., Balasundara prabhu, R., Prasanna, S., Mallick, T. K. & Senthilarasu, S. Review on natural dye sensitized solar cells: Operation, materials and methods. *Renew. and Sust. Energy Rev.* **51**, 1306–1325 (2015).
22. Koyama, Y., Miki, T., Wang, X.-F. & Nagae, H. Dye-Sensitized Solar Cells Based on the Principles and Materials of Photosynthesis: Mechanisms of Suppression and Enhancement of Photocurrent and Conversion Efficiency. *Int. J. Mol. Sci.* **10**, 4575–4622 (2009).
23. Milot, R. L., Moore, G. F., Crabtree, R. H., Brudvig, G. W. & Schmittenmaer, C. A. Electron Injection Dynamics from Photoexcited Porphyrin Dyes into SnO<sub>2</sub> and TiO<sub>2</sub> Nanoparticles. *The J. Phys. Chem. C* **117**, 21662–21670 (2013).
24. Watson, D. F. & Meyer, G. J. Electron injection at dye-sensitized semiconductor electrodes. *Annu Rev Phys Chem.* **56**, 119–156 (2005).
25. Tiwana, P., Parkinson, P., Johnston, M. B., Snaith, H. J. & Herz, L. M. Ultrafast Terahertz Conductivity Dynamics in Mesoporous TiO<sub>2</sub>: Influence of Dye Sensitization and Surface Treatment in Solid-State Dye-Sensitized Solar Cells. *The J. of Phys. Chem.* **114**, 1365–1371 (2010).
26. Nemeč, H. *et al.* Ultrafast terahertz photoconductivity in nanocrystalline mesoporous TiO<sub>2</sub> films. *App. Physics Lett.* **96**, 0621031–0621033 (2010).
27. Koshiya, S., Yamashita, S. & Kimoto, K. Microscopic observation of dye molecules for solar cells on a titania surface. *Sci Rep.* **6**, 24616 (2016).
28. Nazeeruddin, M. K., Humphry-Baker, R., Liska, P. & Grätzel, M. Investigation of Sensitizer Adsorption and the Influence of Protons on Current and Voltage of a Dye-Sensitized Nanocrystalline TiO<sub>2</sub> Solar Cell. *The J. of Phys. Chem. B* **107**, 8981–8987 (2003).
29. Nazeeruddin, M. K., Klein, C., Liska, P. & Grätzel, M. Synthesis of novel ruthenium sensitizers and their application in dye-sensitized solar cells. *Coord Chem. Rev.* **249**, 1460–1467 (2005).
30. Hug, H., Bader, M., Mair, P. & Glatzel, T. Biophotovoltaics: Natural pigments in dye-sensitized solar cells. *Appl. Energy* **115**, 216–225 (2014).
31. Hao, S., Wu, J., Huang, Y. & Lin, J. Natural dyes as photosensitizers for dye-sensitized solar cell. *Sol. Energy* **80**, 209–214 (2006).
32. Hosseinneshad, M., Moradian, S. & Gharanjig, K. Fruit extract dyes as photosensitizers in solar cells. *Cur. Sci.* **109**, 953–956 (2015).
33. Chen, Y. *et al.* THz spectroscopic investigation of 2,4-dinitrotoluene. *Chem. Phys. Lett.* **400**, 357–361 (2004).

34. Yu, B. *et al.* Torsional vibrational modes of tryptophan studied by terahertz time-domain spectroscopy. *Biophys J* **86**, 1649–1654 (2004).
35. Amadi, L. *et al.* Creation of Natural Dye Sensitized Solar Cell Using Nanostructured Titanium Oxide. *Nanosci. Nanoeng.* **3**, 25–35 (2015).

### Acknowledgements

The work was financially supported by the University of Maryland System (Wilson E. Elkins Professorship), Constellation, an Exelon Company (E<sup>2</sup>- Energy to Educate grant program) and Dept of Education (SAFRA Title III Grant). The authors are also grateful to the Institution of Advancement, Coppin State University, for administrative help. The content is exclusively the responsibility of the authors and does not necessarily represent the official views of the funding agencies.

### Author Contributions

J.U. and Anis R. conceived the idea and reviewed the final manuscript. W.G. and Aunik R. designed the experiments. W.G. performed the experiments and wrote the manuscript with the assistance of J.U. All authors participated in the discussion and commented on the paper.

### Additional Information

**Supplementary information** accompanies this paper at <http://www.nature.com/srep>

**Competing financial interests:** The authors declare no competing financial interests.

**How to cite this article:** Ghann, W. *et al.* Interaction of Sensitizing Dyes with Nanostructured TiO<sub>2</sub> Film in Dye-Sensitized Solar Cells Using Terahertz Spectroscopy. *Sci. Rep.* **6**, 30140; doi: 10.1038/srep30140 (2016).



This work is licensed under a Creative Commons Attribution 4.0 International License. The images or other third party material in this article are included in the article's Creative Commons license, unless indicated otherwise in the credit line; if the material is not included under the Creative Commons license, users will need to obtain permission from the license holder to reproduce the material. To view a copy of this license, visit <http://creativecommons.org/licenses/by/4.0/>